RSC Advances

ROYAL SOCIETY OF CHEMISTRY

www.rsc.org/advances

RSC Advances

RSCPublishing

ARTICLE

Improved Thermal Dehydrogenation of Ammonia Borane by MOF-5

Cite this: DOI: 10.1039/x0xx00000x

Zhongyue Li,*[a] Wei Liu,[b] Huijuan Yang,[a] Tai Sun,[c] Kun Liu,[a] Zhenhui Wang,[a] Chao Niu[a]

Received 00th January 2012,
Accepted 00th January 2012

DOI: 10.1039/x0xx00000x

www.rsc.org/

A composite material with ammonia borane (AB) and MOF-5 has been synthesized by infusion method. The decomposition temperature greatly reduces compared with pristine AB. The TPD-MS onset and peak temperature of AB dehydrogenation was 60 ℃ and 84 ℃, respectively. The hydrogen release rate of AB inside MOF-5 was remarkably increased at a safe temperature 85 ℃. The activation energies of AB/MOF-5 is 68.45 kJ·mol^{-1}. The formation of main undesirable volatile byproducts borazine and diborane was prevented. However, ammonia still released during dehydrogenation for the lack of unsaturated coordinated metal in MOF-5. The mechanism of inhibiting ammonia evolution from AB in AB/MOFs system has been taken into clear by comparing AB/MOF-5 with AB/JUC-32-Y. It is suggested that the unsaturated coordinated metal sites play the key role in preventing the escape of ammonia.

1. Introduction

As a promising solid-state hydrogen source material candidate, Ammonia borane (AB) has received much attention due to its remarkable high stoichiometric hydrogen content (19.6 wt%), stable solid phase at room temperature and moderate dehydrogenation conditions.[1] At present, thermolysis and solvolysis (including acid- and metal-catalyzed) are typically approaches to release hydrogen from AB.[2] However, the poor dehydrogenation kinetics of AB is poor below 100 ℃ and the formation of undesirable volatile byproducts, such as borazine ($B_3H_6N_3$), ammonia (NH_3), and diborane (B_2H_6), during dehydrogenation stop the practical application of AB in fuel-cell.[3] Recently, many different methods, such as nanoscaffolds,[4] metal substitution,[5] metallic catalysis,[6] acid catalysis,[7] composite with carbon material,[8-11] ionic liquids,[12] extremely high pressure treatment.[13] etc., had been adopted to improve the thermal dehydrogenation properties of AB. The hydrogen release kinetics has been significantly increased as reported in these references. Our previous research indicated that metal organic frameworks (MOFs) were promising candidates to accelerate dehydrogenation kinetics at a lower temperature and suppress volatile byproduct.[14] MOFs are a kind of novel porous materials constructed with metal centers and organic ligands through coordination bonds. They got a lot of attention due to their multiple skeleton structures, high surface area and modifiable porous properties.[15-18] Recently, several kinds of MOFs confined AB systems have been reported.[19-25] But the mechanisms of how MOFs improve the thermal dehydrogenation of AB, especially the interaction between unsaturated coordinated metal sites and the avoiding of ammonia gas, are not clearly. It is suggested that the unsaturated coordinated metal sites exist in the MOFs may prevent releasing of ammonia in AB/MOFs system. However, the detail mechanism of how the unsaturated coordinated metal sites interact with AB is not clear.[14, 23] Jeong, H. M. etc. reported AB@MOF-5 thermal dehydrogenation system, but NH_3 releasing was not found and the important effect of the unsaturated coordinated metal sites of MOFs in AB-MOFs system was not mentioned.[26] However, the formation of NH_3 is

an important issue because even a small amount of NH_3 poisons the catalysts of proton exchange membrane fuel cells.

In this paper, an AB and MOF-5 (denoted as AB/MOF-5) composite has been synthesized by infusion method. MOF-5 was selected because it was a classical one in MOFs family, which was constructed by the metal ZnO_4 tetrahedron nodes and the rigid organic ligand terephthalic. It has a three-dimensional (3D) permanent porous skeleton with cuboidal pores, high surface area, well-understood synthesis methods.[27~29] Unlike JUC-32-Y, MOF-5 does not have unsaturated coordinated metal sites. Compared with pristine AB, the dehydrogenation temperature of AB/MOF-5 reduced obviously and the dehydrogenation kinetics increased remarkably. The formations of volatile byproducts $B_3H_6N_3$ and B_2H_6 are avoided, but NH_3 still exists in the gas-state products during thermal decomposition. The solid-state ^{11}B NMR studies show that the failure to avoid ammonia gas may due to the absence of unsaturated coordinated metal sites in MOF-5.

2. Experimental

2.1 Sample preparation

MOF-5 synthesis: a mixture of zinc nitrate hexahydrate (0.45 g, 1.5 mmol) and 1,4-benzenedicarboxylic acid (0.083 g, 0.50 mmol) were dissolved in 49 mL *N,N'*-dimethylformamide and 1 mL H_2O at room temperature. The reaction mixture was left in an oven at 100 ℃ for 7 hours to yield cube-shaped crystals. The product was purified and activated as follow: the collected crystals were washed six times with 50 mL of anhydrous CH_3OH. The crystals were soaked in anhydrous CH_3OH for 24 h each time. Then the solvent was toppled. The sample was treated under vacuum at 100 °C for 12 hours to remove the solvent molecules in pores of MOF-5. The activated sample was kept in the glove box with argon.

AB/MOF-5 synthesis: AB/MOF-5 was prepared by dipping method. Activated MOF-5 was added into AB anhydrous methanol solution (0.5 mol/L) with the 1:1 mol ratio of AB:Zn in glove box. Then the mixture was stirred for two hours under an argon atmosphere. The solvent was removed by vacuum at 25 °C. The dry solid AB/MOF-5 was obtained and kept in the glove box with argon.

2.2 Characterization

Powder X-ray diffraction (PXRD) data were collected on a Bruker D8 Advance X-ray diffractometer (Cu-Kα radiation) diffractometer. The voltage and the current were set to be 40kV and 40mA, respectively. Measuring 2θ range is from 4° to 40°. Scan speed is 6°/min. The fourier transform infrared (FTIR) spectra were recorded (4000 - 400 cm^{-1} region) on a Bruker Optics VERTEX 70 Fourier Transform Infrared spectrometer using KBr pellet. N_2 adsorption and desorption were performed on Quantachrome Autosorb-1C at 77 K. CO_2 adsorption was performed on Quantachrome Autosorb-1C at 273 K. Differential scanning calorimetry (DSC) of the samples was carried out using a STA 449 F3 Jupite instrument under argon with a heating rate of 3 °C·min^{-1}. Temperature-programmed desorption mass spectrometry (TPD-MS) data were detected by Micromeritics Chemisorb 2720 and Prismaplus QMG300. The temperature was raised from room temperature to 200 °C at the rate of 3 °C/min, with Ar flowing at a rate of 50 mL/min. Dehydrogenation rate was detected by AMC Gas Reaction Controller. Solid-state ^{11}B NMR spectral experiments were performed on a Varian Infinity-plus 400 spectrometer operating at 128 MHz.

3. Results and discussion

The PXRD pattern of MOF-5 (Figure 1) synthesized sample agrees well with the simulated one. [28] The skeleton structure of MOF-5 maintains after AB is loaded (AB/MOF-5 pattern) and the thermal decomposition at 200 °C for 1 hour as shown in the result of AB/MOF-5-after. The PXRD pattern of AB/MOF-5 does not show any peaks of pristine AB, suggesting the very fine size and well-distributed of AB particles. BET surface area from the N_2 adsorption/desorption data (Figure 2) obviously reduces to 1 $m^2 \cdot g^{-1}$ from 1032 $m^2 \cdot g^{-1}$ after AB loading. And the total pore volume reduces from 0.57 $cm^{-3} \cdot g^{-1}$ to 0.01 as well.

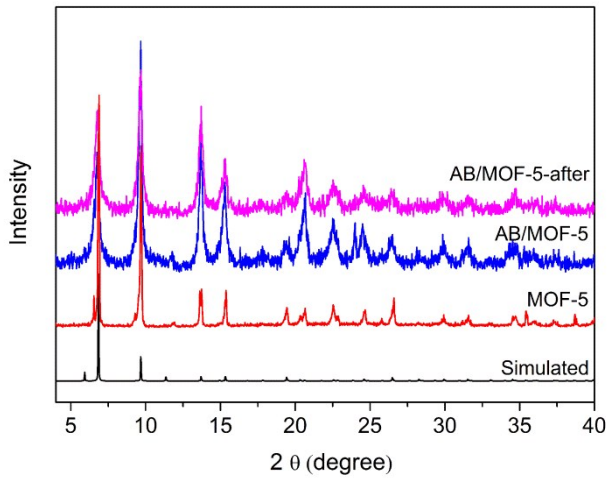

Figure 1. Powder XRD pattern of MOF-5 simulated (black), MOF-5 synthesized (red), AB loaded MOF-5 (AB/MOF-5, blue) and afer dehydrogenation at 200 °C for 1 hour (AB/MOF-5-after, purple).

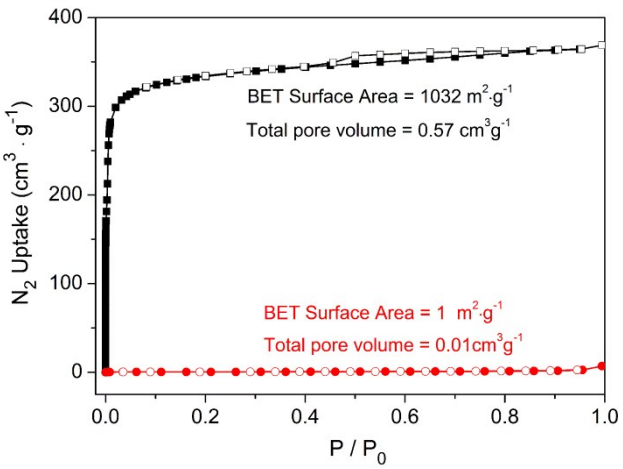

Figure 2. N_2 adsorption (solid) and desorption (dashed) isotherm of MOF-5 (square) and AB/MOF-5 (circle) at 77 K.

The N_2 adsorption/desorption data shows that the pores of MOF-5 are almost occupied by AB particles. The FTIR spectra of pristine AB, MOF-5, AB/MOF-5 and AB/MOF-5-after were shown in Figure 3. Comparing with MOF-5 synthesized, some new bands at 3311, 3195, 2279, 1059, 782 cm^{-1}, attributable to the H-N antisymmetric stretching, H-N symmetric stretching, H-B symmetric stretching, H wagging and B-N stretching,[30] in AB loaded MOF-5 sample were observed. After heated at 200 °C for 1 hour, all the H-N stretching, H-B stretching, H wagging and B-N stretching disappear in AB/MOF-5-after sample. It indicates that the

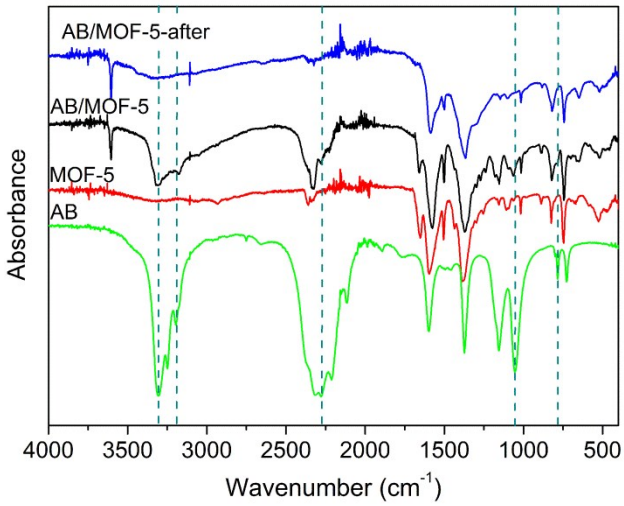

Figure 3. FTIR spectra of pristine AB (green), MOF-5 synthesized (red), AB/MOF-5 (black) and AB/MOF-5-after (blue).

dehydrogenation reaction is completed and B-N bond is broken after heated at 200 °C for 1 hour.

The pyrolysis behavior of AB/MOF-5 was investigated through TPD-MS and dehydrogenation rate. TPD-MS (Figure 4) shows the mass profiles of the main volatile products (H_2, NH_3, B_3H_6 and $B_3H_6N_3$) released from AB. The onset dehydrogenation temperature of AB/MOF-5 decrease to 60 °C .The peak releasing temperature is c.a. 84 °C, while the one of pristine AB is 114 °C. A similar improvement in AB/JUC-32-Y composite system was reported in our early studied.[14] The porous structure and metal containing help decrease the decomposition temperature and speed up the H_2 release rate. The absence of signal peak of 27 and 80 for AB/MOF-5 indicate that loading AB into MOF-5 could suppress the emission of diborane and borazine. However, a peak of 17 belongs to ammonia was detected during the dehydrogenation. By contrast, AB/JUC-32-Y can avoid the emission of ammonia completely. The difference between the structure of MOF-5 and JUC-32-Y is that the metal Zn^{2+} of MOF-5 is saturated coordinated with carboxyl, while the Y^{3+} in treated JUC-32-Y is unsaturated coordinated. Thus, it is supposed that MOF-5 lacks the unsaturated metal in its structure to prevent the evolution of ammonia during AB pyrolysis. Solid-state ^{11}B NMR of the samples were shown in Figure 5. ^{11}B resonance in the AB/MOF-5 exhibits a same chemical shift at -22.8 p.p.m. as in pristine AB,[31]

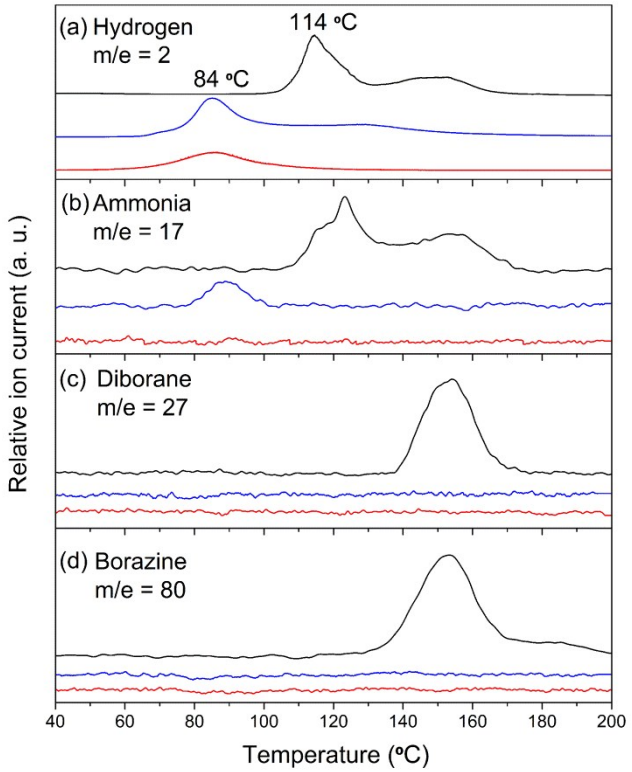

Figure 4. TPD-MS spectra of pristine AB (black), AB/MOF-5 (blue) and AB/JUC-32-Y (red).

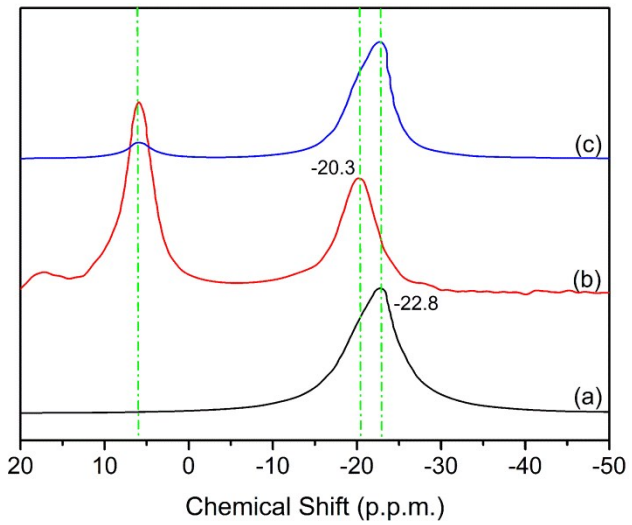

Figure 5. Solid–state ^{11}B NMR of (a) pristine AB, (b) AB/JUC-32-Y, (c) AB/MOF-5.

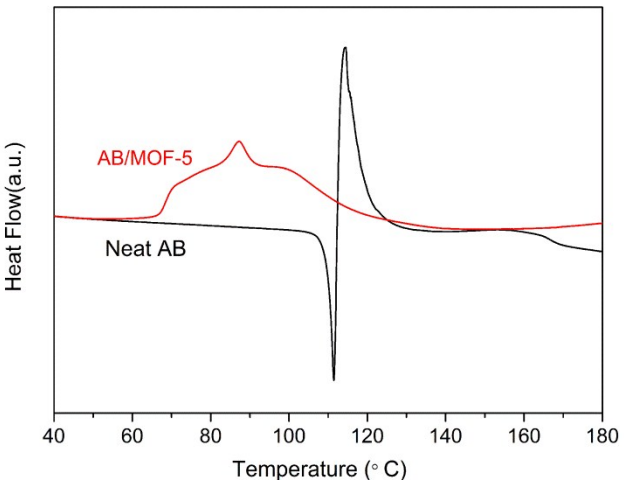

Figure 6. DSC profiles of neat AB and AB/MOF-5 with a heating rate of 3 ℃ min^{-1}.

while the AB/JUC-32-Y shows a downfield shift at -20.3 p.p.m. It is suggested that the unsaturated coordinated Y^{3+} of AB/JUC-32-Y as a Lewis acid site may interact with -NH_3 in AB which has electron donor property. As a result, N atoms are bound at the framework of JUC-32-Y, so there is no NH_3 escaping during AB/JUC-32-Y thermolysis. Saturated coordinated metal center Zn^{2+} in MOF-5 cannot form the binding effect with N atom of AB, so that NH_3 still exists in the gas product. $ZnCl_2$ has been reported as an effective material to suppress the emission of NH_3 during AB pyrolysis.[32] The stable saturated coordination configuration may invalidate the Zn^{2+} in MOF-5 to do the job. The additional chemical shift at 6.0 p.p.m. in AB/JUC-32-Y and AB/MOF-5 should be ascribed to the formation of B-O band.[33] which prevents the release of byproduct containing B atom during thermolysis.

The differential scanning calorimetry (DSC) results of AB/MOF-5 compared with neat AB are shown in Figure 6. Neat AB shows an endothermic dip at ~110 ° C assigned to its melting at ~110 ℃ and two exothermic peaks associated with the release of hydrogen at ~ 114 ° C and ~ 158 ° C, respectively. AB/MOF-5 expresses only exothermic peaks at 87 ° C, which is attributed to its thermal decomposition.

Figure 7. shows the dehydrogenation rate of the samples at 75 ° C, 85 ° C, 95 ° C and 105 ° C., AB/MOF-5 shows much better dehydrogenation kinetics than that of pristine AB. At 85 ° C pristine AB scarcely releases any H_2. H_2 uptake of AB inside MOF-5 is 3.6 wt%, 5.1 wt%, 6.6 wt%, 8.9 wt% within 20 min and reach 4.7 wt%, 5.9 wt%, 7.1 wt%, 9.2 wt% in 60 min, respectively. The dehydrogenation activation energies have been calculated through Arrhenius equation. From the slope of the linear plot of lnk versus 1/T, the Arrhenius activation energies for H_2 release from AB/MOF-5 is 68.45

kJ·mol^{-1}, which is obviously less than that of pristine AB (135.0 kJ·mol^{-1}).[9]

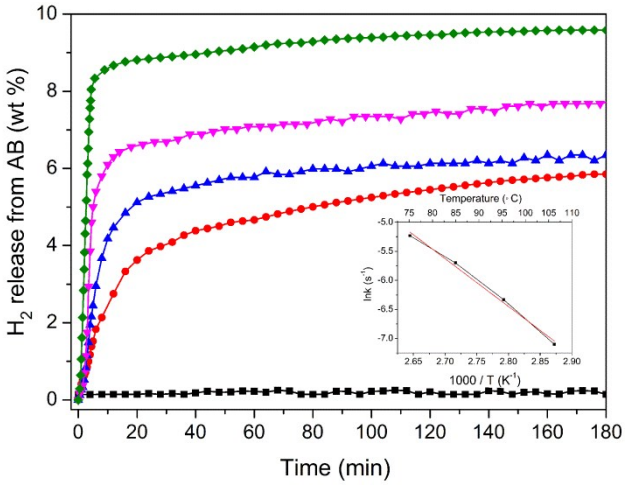

Figure 7. Hydrogen desorption from pristine AB (black) at 85 °C and AB/MOF-5 at 75 °C (red), 85 °C (blue), 95 °C (purple) and 105 °C (green). The inset is the linear plot of lnk versus 1/T of AB/MOF-5.

It is proposed that (1) the porous structure and metal containing are helpful to decrease the decomposition temperature and accelerate the H_2 release rate. Big surface area could prevent the formation of $B_3H_6N_3$; (2) the unsaturated coordinated metal site is the key factor to avoid the formation of volatile byproduct NH_3 gas in AB/MOFs system. (3) O atom of carboxyl contributes to inhibit B_2H_6 evolution from AB.

Conclusions

In this paper, we have demonstrated that MOF-5 is an effective carrier material to improve thermal dehydrogenation of AB. Both the onset and peak dehydrogenation temperature were decreased obviously. The H_2 releasing rate of AB loaded into MOF-5 was improved. However, MOF-5 was not effective as JUC-32-Y to prevent the undesirable volatile byproduct. MOF-5 could avoid the escaping of $B_3H_6N_3$ and B_2H_6 successfully, but it failed to prevent the forming of NH_3 gas. The saturated coordinated metal center Zn^{2+} in MOF-5 cannot interact with N atoms of AB, so that N cannot be bind at the framework of MOF-5. The solid-state ^{11}B NMR investigation explained the key factor of unsaturated coordinated metal sites for preventing the escaping of undesirable volatile byproduct ammonia. Although AB/MOF-5 did not exhibit much superiority in hydrogen release rate and gas byproducts formation, but the mechanisms of AB/MOFs dehydrogenation system have been discussed deeply, especially for the preventing of NH_3 emission. It is significative for knowing AB/MOFs system clearly and finding more efficient AB dehydrogenation system to apply it into industry and transportation.

Acknowledgements

This work was supported by the National Natural Science Foundation of China (No. 21101059, 51101037), PhD Fund of Henan Polytechnic University (B2011-030), Pearl River Science and Technology Scholar Project of Guangzhou (2014J2200094), Guangdong Scientific research project (2013B010403018) and Key Cultivation Foundation for Fundamental Research of Henan University of Technology(2013JCYJ02).

Notes and references

[a] Department of Physics-Chemistry, Henan Polytechnic University, Jiaozuo, 454000, China. Email: lizhongyue@hpu.edu.cn

[b] School of Mechanical & Electrical Engineering, Henan University of Technology, Zhengzhou, 450007, China.

[c] Guangdong Province Key Laboratory of Rare Earth Development and Application, Guangdong Research Institute of Industrial Technology, Guangzhou, 510650, China.

1 Z. T. Xiong, C. K. Yong, G.T. Wu, P. Chen, W. Shaw, A. Karkamkar, T. Autrey, M. O. Jones, S. R. Johnson, P. P. Edwards, W. F David, *Nat. Mater*, 2008, **7**, 138-141.

2 C. W. Hamilton, R. T. Baker, A. Staubitzc, I. Manners, *Chem. Soc. Rev.*, 2009, **38**, 279–293.

3 S. Gadipelli, J. Ford, W. Zhou, H. Wu, T. J. Udovic, T. Yildirim, *Chem. Eur. J.*, 2011, **17**, 6043 – 6047.

4 A. Gutowska, L. Li, Y. S. Shin, C. M. Wang, X. H. S. Li, J. C. Linehan, R. S. Smith, B. D. Kay, B. Schmid, W. Shaw, M. Gutowski, T. Autrey, *Angew. Chem. Int. Ed.*, 2005, **44**, 3578-3582.

5 Z. T. Xiong, G. T. Wu, Y. S. Chua, J. J. Hu, T. He, W. L. Xu, P. Chen, *Energy. Environ. Sci.*, 2008, **1**, 360-363.

6 M. C. Denney, V. Pons, T. J. Hebden, D. M. Heinekey, K. I. Goldberg, *J. Am. Chem. Soc*.,2006, **128**, 9582–9583.

7 F. H. Stephens, R. T. Baker, M. H. Matus, D. J. Grant, D. A. Dixon, *Angew. Chem. Int. Ed.*, 2007, **46**, 746–749.

8 X. W. Chen, L. Wan, J. M. Huang, L. Z. Ouyang, M. Zhu, Z. P. Guo, X. B. Yu, *Carbon*, 2014, **68**, 462–472.

9 Z. W. Tang, H. Chen, X. W. Chen, L. M. Wu, X. B. Yu, *J. Am. Chem. Soc.*, 2012, **134**, 5464−5467.

10 G. Moussa, S. Bernard, U. B. Demirci, R. Chiriac, P. Miele, *Int. J. Hydrogen. Energ.*, 2012, **37**, 13437−13445.

11 Z. W. Tang, X.W. Chen, H. Chen, L. M. Wu, X. B. Yu, *Angew. Chem. Int. Ed.*, 2013, **52**, 5832−5835.

12 M. E. Bluhm, M. G. Bradley, R. Butterick, U. Kusari, L. G. Sneddon, *J. Am. Chem. Soc*., 2006, **128**, 7748–7749.

13 Y. Lin, W. L. Mao, H. K. Mao, *Proc. Natl. Sci.*, 2009, **106**, 8113-8116.

14 Z. Y. Li, G. S. Zhu, G. Q. Lu, S. L. Qiu, X. D. Yao, *J. Am. Chem. Soc.* , 2010, **132**, 1490–1491.

15 H. Li, M. Eddaoudi, M. O'Keeffe, O. M. Yaghi, *Nature*, 1999, **402**, 276-279.

16 A. R. Millward, O. M. Yaghi, *J. Am. Chem. Soc.***,** 2005, **127**, 17998-17999.

17 A. L. Grzesiak, F. J. Uribe, N. W. Ockwig, O. M. Yaghi, A. J. Matzger, *Angew. Chem. Int. Ed.*, 2006, **45**, 2553 – 2556.

18 G. Férey, C. Mellot-Draznieks, C. Serre, F. Millange, J. Dutour, S. Surblé, I. Margiolaki, *Science*, 2005, **309**, 2040-2042.

19 G. Srinivas, J. Ford, W. Zhou, T. Yildirim, *Int. J. Hydrogen. Energ.*, 2012, **37**, 3633-3638.

20 X. L. Si, L. X. Sun, F. Xu, C. L. Jiao, F. Li, S. S. Liu, J. Zhang, L. F. Song, C. H. Jiang, S. Wang, Y. L. Liu, Y. Sawada, *Int. J. Hydrogen. Energ.*, 2011, **36**, 6698-6704.

21 Q. L. Zhu, J. Li, Q. Xu, *J. Am. Chem. Soc.*, 2013, **135**, 10210−10213.

22 R. Q. Zhong, R. Q. Zou, T. Nakagawa, M. Janicke, T. A. Semelsberger, A. K. Burrell, R. E. D. Sesto, *Inorg. Chem*., 2012, 51, 2728−2730.

23 G. Srinivas, W. Travis, J. Ford, H. Wu, Z. X. Guo, T. Yildirim, *J. Mater. Chem. A*, 2013, **1**, 4167−4172.

24 L. Gao, C. Y. Vanessa Li, H. Yung, K. Y. Chan, *Chem. Commun.*, 2013, **49**, 10629−10631.

25 S. Gadipelli, J. Ford, W. Zhou, H. Wu, T. J. Udovic, T. Yildirim, *Chem. Eur. J*., 2011, **17**, 6043−6047.

26 H. M. Jeong, W.H. Shin, J. H. Park, J. H. Choi, J. Ku Kang, *Nanoscale*, 2014, **6**, 6526–6530.

27 H. L. Li, M. Eddaoudi, M. O'Keeffe, O. M. Yaghi, *Nature*, 1999, **402**, 276–279.

28 S. S. Kaye, A. Dailly, O. M. Yaghi, J. R. Long, *J. Am. Chem. Soc*., 2007, **129**, 14176–14177.

29 B. Panella, M. Hirscher, *Adv. Mater*., 2005, **17**, 538–541.

30 S. M. Lee, X. D. Kang, P Wang,. H. M. Cheng, Y. H. Lee, *Chemphyschem*, 2009, **10**, 1825–1833.

31 D. W. Himmelberger, C. W. Yoon, M. E. Bluhm, P. J. Carroll, L. G. Sneddon, *J. Am. Chem. Soc.*, 2009, **131**, 14101–14110.

32 S. F. Li, Z. W. Tang, Y. B. Tan, X. B. Yu, *J. Phys. Chem. C*, 2012, **116**, 1544–1549.

33 S. Sepehri, A. Feaver, W. J. Shaw, C. J. Howard, Q. F. Zhang, T. Autrey, G. Z. Cao, *J. Phys. Chem. B*, 2007, **111**, 14285–14289.

